

Direct observation of spin-polarized surface states in the parent compound of a topological insulator using spin-resolved-ARPES spectroscopy in a Mott-polarimetry mode

D. Hsieh,¹ L. Wray,¹ D. Qian,¹ Y. Xia,¹ Y.S. Hor,² R.J. Cava,² and M.Z. Hasan^{1,3}

¹*Joseph Henry Laboratories : Department of Physics,
Princeton University, Princeton, NJ 08544, USA*

²*Department of Chemistry, Princeton University, Princeton, NJ 08544, USA*

³*Princeton Center for Complex Materials, Princeton University, Princeton, NJ 08544, USA*

(Dated: November 5, 2021)

We report high-resolution spin-resolved photoemission spectroscopy (Spin-ARPES) measurements on the parent compound Sb of the recently discovered 3D topological insulator $\text{Bi}_{1-x}\text{Sb}_x$ [D. Hsieh et al., Nature 452, 970 (2008)]. By modulating the incident photon energy, we are able to map both the bulk and (111) surface band structure, from which we directly demonstrate that the surface bands are spin polarized by the spin-orbit interaction and connect the bulk valence and conduction bands in a topologically non-trivial way. A unique asymmetric Dirac surface state gives rise to a k-splitting of its spin polarized electronic channels. These results complement our previously published works on this materials class and re-confirm our discovery of topological insulator states in the $\text{Bi}_{1-x}\text{Sb}_x$ series.

PACS numbers:

Topological insulators are a new phase of quantum matter that are theoretically distinguished from ordinary insulators by a Z_2 topological number that describes its bulk band structure [1–3]. They are characterized by a bulk electronic excitation gap that is opened by spin-orbit coupling, and unusual metallic states that are localized at the boundary of the crystal. The two-dimensional (2D) version, known as the quantum spin Hall insulator [4–6], is commonly understood as two copies of the integer quantum Hall effect [7] where the spin-orbit coupling acts as a magnetic field that points in a spin dependent direction, giving rise to counter propagating spin polarized states [8] on the 1D crystal edge. Three-dimensional topological insulators on the other hand have no quantum Hall analogue. Its surface states, which are necessarily spin polarized, realize a novel 2D metal that remains delocalized even in the presence of disorder [2, 3, 9–11]. For these reasons, they have also been proposed as a route to dissipationless spin currents which, unlike current semiconductor heterostructure based spintronics devices, do not require an externally applied electric field.

Recent photoemission [12] and theoretical results [2, 10] suggest that single crystals of insulating $\text{Bi}_{1-x}\text{Sb}_x$ ($0.07 \leq x \leq 0.22$) alloys realize a 3D topological insulator. The non-trivial Z_2 invariant that characterizes $\text{Bi}_{1-x}\text{Sb}_x$ is inherited from the bulk band structure of pure Sb [2, 10], therefore, although Sb is a bulk semimetal, its non-trivial bulk band topology should be manifest in its surface state spectrum. Such a study requires a separation of the Fermi surface of the surface states of Sb from that of its bulk states over the entire surface Brillouin zone (BZ), as well as a direct measurement of the spin degeneracy of the surface states. To date, angle-resolved photoemission spectroscopy (ARPES) experiments on low lying states have only been performed on single crystal Sb with fixed He

α radiation (apart from our previous work on this), which does not allow for separation of bulk and surface states [13]. Moreover the aforementioned study, as well as ARPES experiments on Sb thin films [14], only map the band dispersion near $\bar{\Gamma}$, missing the band structure near \bar{M} that is critical to determining the Z_2 invariant [12]. In this work, we have performed spin- and angle-resolved photoemission experiments on single crystal Sb(111). Using variable photon energies, we successfully isolate the surface from bulk electronic bands over the entire BZ and map them with spin sensitivity. We show directly that the surface states are gapless and spin split, and that they connect the bulk valence and conduction bands in a topologically non-trivial way.

Spin-integrated ARPES measurements were performed with 14 to 30 eV photons on beam line 5-4 at the SSRL and at ALS BL-12 at higher photon energies. Spin resolved ARPES measurements were performed at the SIS beam line at the SLS using the COPHEE spectrometer [15] with a single 40 kV classical Mott detector and a photon energy of 20 eV. The typical energy and momentum resolution was 15 meV and 1% of the surface BZ respectively at beam line 5-4, and 80 meV and 3% of the surface BZ respectively at SIS using a pass energy of 3 eV. High quality single crystals of Sb and $\text{Sb}_{0.9}\text{Bi}_{0.1}$ were grown by methods detailed in [12]. Cleaving these samples *in situ* between 10 K and 55 K at chamber pressures less than 5×10^{-11} torr resulted in shiny flat surfaces, characterized by low energy electron diffraction to be clean and well ordered with the same symmetry as the bulk [Fig. 1(a) & (b)]. This is consistent with photoelectron diffraction measurements that show no substantial structural relaxation of the Sb(111) surface [16]. Band calculation was performed using the full potential linearized augmented plane wave method in film geometry as implemented in the FLEUR program and local density approximation for

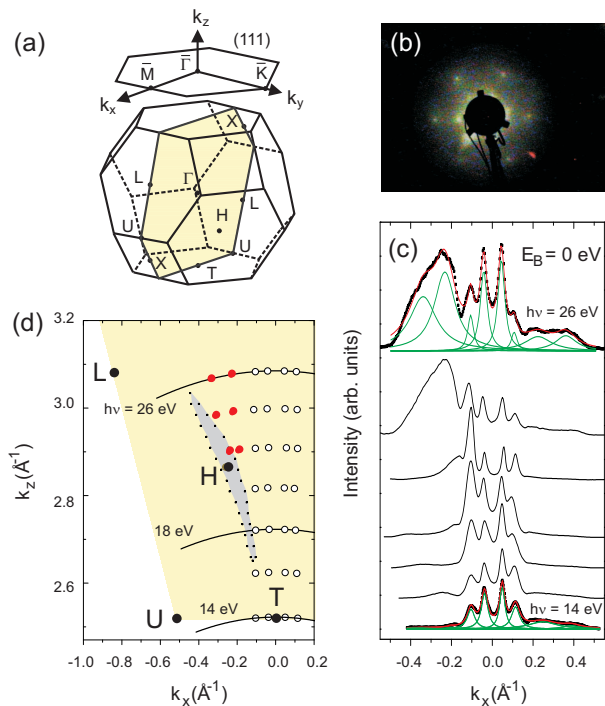


FIG. 1: Experimental separation of bulk from surface electron states in Sb using ARPES. (a) Schematic of the bulk BZ of Sb and its (111) surface BZ. The shaded region denotes the momentum plane in which the following ARPES spectra were measured. (b) LEED image of the *in situ* cleaved (111) surface exhibiting a clear hexagonal symmetry. (c) Select MDCs at the Fermi level taken with photon energies from 14 eV to 26 eV in steps of 2 eV, taken in the *TXLU* momentum plane. Peak positions in the MDCs were determined by fitting to Lorentzians (red curves). (d) Experimental 3D bulk Fermi surface near H (red circles) and 2D surface Fermi surface near $\bar{\Gamma}$ (open circles) determined by matching the fitted peak positions from (c) to calculated constant $h\nu$ contours (black curves). Theoretical hole Fermi surface calculated in [23].

description of the exchange correlation potential [17].

Figure 1(c) shows momentum distributions curves (MDCs) of electrons emitted at E_F as a function of k_x ($\parallel \bar{\Gamma}\bar{M}$) for Sb(111). The out-of-plane component of the momentum k_z was calculated for different incident photon energies ($h\nu$) using the free electron final state approximation with an experimentally determined inner potential of 14.5 eV [14]. There are four peaks in the MDCs centered about $\bar{\Gamma}$ that show no dispersion along k_z and have narrow widths of $\Delta k_x \approx 0.03 \text{ \AA}^{-1}$. These are attributed to surface states and are similar to those that appear in Sb(111) thin films [14]. As $h\nu$ is increased beyond 20 eV, a broad peak appears at $k_x \approx -0.2 \text{ \AA}^{-1}$, outside the k range of the surface states near $\bar{\Gamma}$, and eventually splits into two peaks. Such a strong k_z disper-

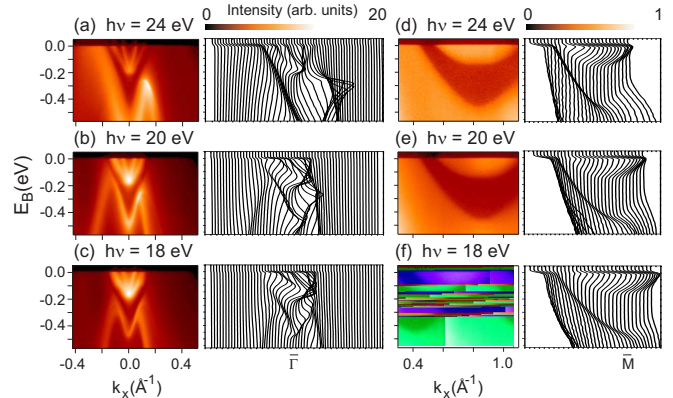


FIG. 2: Surface and bulk band dispersion. ARPES intensity maps as a function of k_x near $\bar{\Gamma}$ (a)-(c) and \bar{M} (d)-(f) and their corresponding EDCs, taken using $h\nu = 24 \text{ eV}$, 20 eV and 18 eV photons. The intensity scale of (d)-(f) is a factor of about twenty smaller than that of (a)-(c) due to the intrinsic weakness of the ARPES signal near \bar{M} .

sion, together with a broadened linewidth ($\Delta k_x \approx 0.12 \text{ \AA}^{-1}$), is indicative of bulk band behavior, and indeed these MDC peaks trace out a Fermi surface [Fig. 1(d)] that is similar in shape to the hole pocket calculated for bulk Sb near H [23]. Therefore by choosing an appropriate photon energy (e.g. $\leq 20 \text{ eV}$), the ARPES spectrum along $\bar{\Gamma}\bar{M}$ will have contributions from only the surface states. The small bulk electron pocket centered at L is not accessed using the photon energy range we employed [Fig. 1(d)].

ARPES spectra along $\bar{\Gamma}\bar{M}$ taken at three different photon energies are shown in Fig. 2. Near $\bar{\Gamma}$ there are two rather linearly dispersive electron like bands that meet exactly at $\bar{\Gamma}$ at a binding energy $E_B \sim -0.2 \text{ eV}$. This behavior is consistent with previous ARPES measurements along the $\bar{\Gamma}\bar{K}$ direction [13] and is thought to come from a pair of spin-split surface bands that become degenerate at the time reversal invariant momentum (TRIM) $\bar{\Gamma}$ due to Kramers degeneracy. The Fermi velocities of the inner and outer V-shaped bands are $4.4 \pm 0.1 \text{ eV}\cdot\text{\AA}$ and $2.2 \pm 0.1 \text{ eV}\cdot\text{\AA}$ respectively as found by fitting straight lines to their MDC peak positions. The surface origin of this pair of bands is established by their lack of dependence on $h\nu$ [Fig. 2(a)-(c)]. A strongly photon energy dispersive hole like band is clearly seen on the negative k_x side of the surface Kramers pair, which crosses E_F for $h\nu = 24 \text{ eV}$ and gives rise to the bulk hole Fermi surface near H [Fig. 1(d)]. For $h\nu \leq 20 \text{ eV}$, this band shows clear back folding near $E_B \approx -0.2 \text{ eV}$ indicating that it has completely sunk below E_F . Further evidence for its bulk origin comes from its close match to band calculations [Fig. 2(a)]. Interestingly, at photon energies such as 18 eV where the bulk bands are far below E_F , there remains a uniform envelope of weak spectral inten-

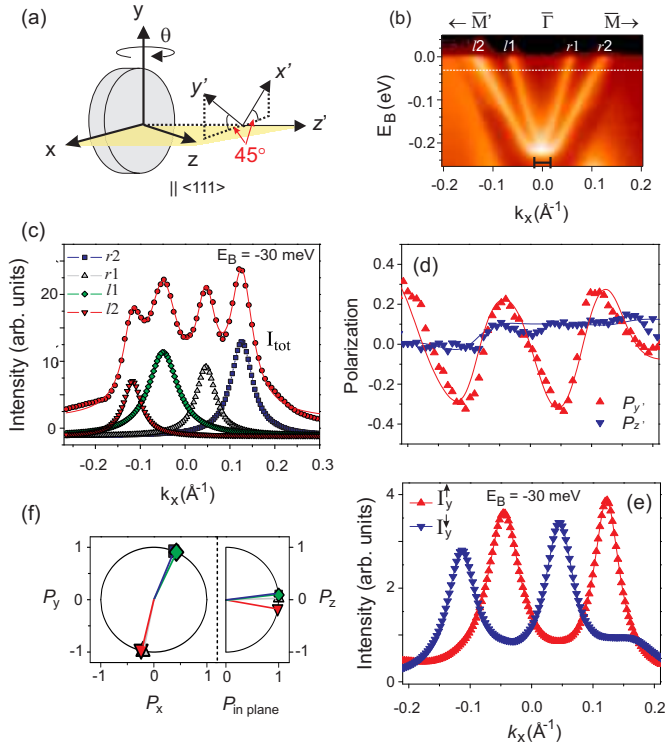


FIG. 3: Large spin splitting of surface states on Sb(111). (a) Experimental geometry of the spin resolved ARPES study. At normal emission ($\theta=0^\circ$), the sensitive y' -axis of the Mott detector is rotated by 45° from the sample $\bar{\Gamma}$ - \bar{M} ($\parallel x$) direction, and the sensitive z' -axis of the Mott detector is parallel to the sample normal. Spin up and down are measured with respect to these two quantization axes. (b) Spin integrated ARPES spectra along the \bar{M}' - $\bar{\Gamma}$ - \bar{M} direction taken using a photon energy $h\nu = 22$ eV. The momentum splitting between the band minima is indicated by the black bar and is approximately 0.03\AA^{-1} . (c) Momentum distribution curve of the spin integrated spectra at $E_B = -30$ meV (shown in (b) by white line) using a photon energy $h\nu = 20$ eV, together with the Lorentzian peaks of the fit. (d) Measured spin polarization curves (symbols) for the y' and z' components together with the fitted lines using the two-step fitting routine. Even though the measured polarization only reaches a magnitude of around ± 0.4 , similar to what is observed in thin film Bi(111) [20], this is due to a non-polarized background and overlap of adjacent peaks with different spin polarization. The fitted parameters are in fact consistent with 100% polarized spins. (e) Spin resolved spectra for the y component based on the fitted spin polarization curves shown in (d). (f) The in-plane and out-of-plane spin polarization components in the sample coordinate frame obtained from the spin polarization fit. The symbols refer to those in (c).

sity near the Fermi level in the shape of the bulk hole pocket seen with $h\nu = 24$ eV photons, which is symmetric about $\bar{\Gamma}$. This envelope does not change shape with $h\nu$ suggesting that it is of surface origin. Due to its weak intensity relative to states at higher binding energy, these features cannot be easily seen in the energy distribution

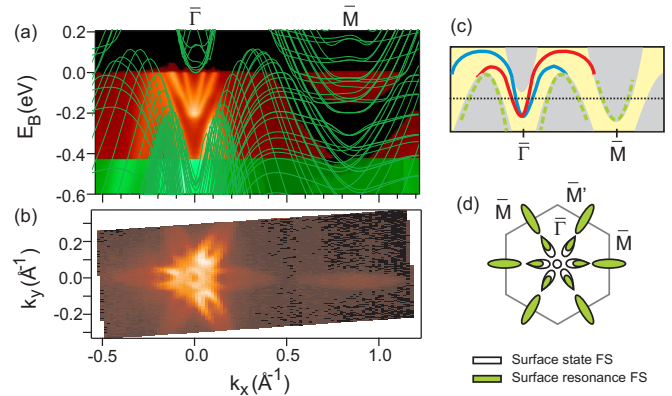


FIG. 4: Topologically non-trivial surface states of Sb(111). (a) Calculated surface state band structure for freestanding 20 bilayer Sb(111) slabs together with an ARPES intensity map of Sb(111) along the $\bar{\Gamma}$ - \bar{M} direction taken with $h\nu = 22$ eV photons. Green curves show the calculated bulk bands along the k_x direction projected onto the (111) plane. (b) ARPES intensity map at E_F in the k_x - k_y plane taken with $h\nu = 20$ eV photons. (c) Schematic picture showing that the gapless spin polarized surface bands (red and blue lines) connect the projected bulk valence and conduction bands (shaded regions) and are thus topologically non-trivial. The surface resonances (dashed green lines) do not connect the bulk valence and conduction bands and are thus topologically trivial. (d) Schematic of the surface Fermi surface topology of Sb(111) showing the pockets formed by the pure surface states (unfilled) and the surface resonances (filled green). The purely surface state Fermi contours enclose only the one surface TRIM located at $\bar{\Gamma}$.

curves (EDCs) in Fig. 2(a)-(c), but can be clearly observed in the MDCs shown in Fig. 1(c) especially on the positive k_x side. Centered about the \bar{M} point, we also observe a crescent shaped envelope of weak intensity that does not disperse with k_z [Fig. 2(d)-(f)], pointing to its surface origin. Unlike the sharp surface states near $\bar{\Gamma}$, the peaks in the EDCs of the feature near \bar{M} are much broader ($\Delta E \sim 80$ meV) than the spectrometer resolution (15 meV). The origin of this diffuse ARPES signal is not due to surface structural disorder because if that were the case, electrons at $\bar{\Gamma}$ should be even more severely scattered from defects than those at \bar{M} . In fact, the occurrence of both sharp and diffuse surface states originates from a k dependent coupling to the bulk as discussed later.

To extract the spin polarization vector of each of the surface bands near $\bar{\Gamma}$, we performed spin resolved MDC measurements along the \bar{M}' - $\bar{\Gamma}$ - \bar{M} cut at $E_B = -30$ meV for maximal intensity, and used the two-step fitting routine developed in [24]. The Mott detector in the COPHEE instrument is mounted so that at normal emission it is sensitive to a purely out-of-plane spin component (z') and a purely in-plane (y') spin component that is rotated by 45° from the sample $\bar{\Gamma}$ - \bar{M} direction [Fig. 3(a)]. Each of these two directions rep-

resents a normal to a scattering plane, defined by the electron incidence direction on a gold foil and two detectors mounted on either side that measure the left-right asymmetry $A_{y',z'} = [(I_L^{y',z'} - I_R^{y',z'}) / (I_L^{y',z'} + I_R^{y',z'})]$ of electrons backscattered off the gold foil [15]. Figure 3(d) shows the spin polarization for both components given by $P = (1/S_{eff}) \times A_{y',z'}$, where $S_{eff} = 0.085$ is the Sherman function. Following the procedure described in [24], we take the spins to be fully polarized, assign a spin resolved spectra for each of the fitted peaks I^i shown in Fig. 3(c), and fit the calculated polarization spectrum to measurement. The spin resolved spectra for the y component derived from the polarization fit is shown in Fig. 3(e), given by $I_y^{\uparrow,\downarrow} = \sum_{i=1}^4 I^i (1 \pm P_y^i) / 6 + B / 6$, where B is a background and P_y^i is the fitted y component of polarization. There is a clear difference in I_y^{\uparrow} and I_y^{\downarrow} at each of the four MDC peaks indicating that the surface state bands are spin polarized. Each of the pairs $l2/l1$ and $r1/r2$ have opposite spin, consistent with the behavior of a spin split Kramers pair, and the spin polarization of these bands are reversed on either side of $\bar{\Gamma}$ in accordance with time reversal symmetry [Fig. 3(f)]. Similar to Au(111) [21] and W(110)-(1×1)H [18], the spin polarization of each band is largely in-plane consistent with a predominantly out-of-plane electric field at the surface. However unlike the case in Au(111), where the surface band dispersion is free electron like and the magnitude of the Rashba coupling can be quantified by the momentum displacement between the spin up and spin down band minima [21], the surface band dispersion of Sb(111) is highly non-parabolic. A comparison of the k -separation between spin split band minima near $\bar{\Gamma}$ of Sb(111) [Fig. 3(b)] with those of Bi(111) [17], which are 0.03 \AA^{-1} and 0.08 \AA^{-1} respectively, nevertheless are consistent with the difference in their atomic p level splitting of Sb(0.6 eV) and Bi(1.5 eV) [25]. Therefore, despite Sb having a similar atomic spin-orbit coupling strength to Au(0.5 eV), the k splitting between spin polarized surface bands near E_F is greater in Sb due to its unique dispersion. This could also be due to the nature of spin-polarized photoemission and detection methods.

Figure 4(a) shows the full ARPES intensity map from $\bar{\Gamma}$ to \bar{M} together with the calculated bulk bands of Sb projected onto the (111) surface. Although the six-fold rotational symmetry of the surface band dispersion is not known *a priori* due to the three-fold symmetry of the bulk, we measured an identical surface band dispersion along $\bar{\Gamma}$ - \bar{M} . The spin-split Kramers pair near $\bar{\Gamma}$ lie completely within the gap of the projected bulk bands near E_F attesting to their purely surface character. In contrast, the weak diffuse hole like band centered near $k_x = 0.3 \text{ \AA}^{-1}$ and electron like band centered near $k_x = 0.8 \text{ \AA}^{-1}$ lie completely within the projected bulk valence and conduction bands respectively, and thus their ARPES spectra exhibit the expected lifetime broadening due to coupling with the underlying bulk continuum [26]. Figure 4(b) shows the ARPES intensity plot at E_F of Sb(111) taken at a photon energy of 20 eV, where the

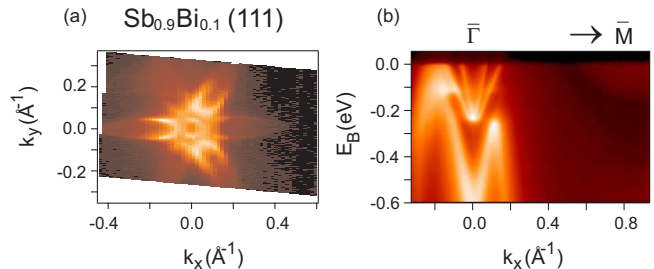


FIG. 5: Spin split surface states survive alloying disorder in $\text{Sb}_{0.9}\text{Bi}_{0.1}$. (a) ARPES intensity map at E_F of single crystal $\text{Sb}_{0.9}\text{Bi}_{0.1}(111)$ in the k_x - k_y plane taken using 20 eV photons. (b) ARPES intensity map of $\text{Sb}_{0.9}\text{Bi}_{0.1}(111)$ along the $\bar{\Gamma}$ - \bar{M} direction taken with $h\nu = 22$ eV photons.

bulk band near H is completely below E_F [Fig. 2(b)]. Therefore this intensity map depicts the topology of the Fermi surface due solely to the surface states. By comparing Figs 4(a) and (b), we see that the inner most spin polarized V-shaped band produces the circular electron Fermi surface enclosing $\bar{\Gamma}$ while the outer spin polarized V-shaped band produces the inner segment ($0.1 \text{ \AA}^{-1} \leq k_x \leq 0.15 \text{ \AA}^{-1}$) of the six hole Fermi surfaces away from $\bar{\Gamma}$. Previous ARPES experiments along the $\bar{\Gamma}$ - \bar{K} direction [13] show that this outer V-shaped band merges with the bulk valence band, however the exact value of k_x where this occurs along the $\bar{\Gamma}$ - \bar{M} direction is unclear since only occupied states are imaged by ARPES. The outer segment of the six hole pockets is formed by the hole like surface resonance state for $0.15 \text{ \AA}^{-1} \leq k_x \leq 0.4 \text{ \AA}^{-1}$. In addition, there are electron Fermi surfaces enclosing \bar{M} and \bar{M}' produced by surface resonance states at the BZ boundaries. Altogether, these results show that in a single surface BZ, the bulk valence and conduction bands are connected by a lone Kramers pair of surface states [Fig. 4(c)].

In general, the spin degeneracy of surface bands on spin-orbit coupled insulators can be lifted due to the breaking of space inversion symmetry. However Kramers theorem requires that they remain degenerate at four special time reversal invariant momenta (TRIM) on the 2D surface BZ, which for Sb(111) are located at $\bar{\Gamma}$ and three \bar{M} points rotated by 60° from one another. According to recent theory, there are a total of four Z_2 topological numbers $\nu_0; (\nu_1 \nu_2 \nu_3)$ that characterize a 3D spin-orbit coupled insulator's bulk band structure [3, 9, 11]. One in particular (ν_0) determines whether the spin polarized surface bands cross E_F an even or odd number of times between any pair of surface TRIM, and consequently whether the insulator is trivial ($\nu_0=0$) or topological ($\nu_0=1$). An experimental signature of topologically non-trivial surface states in insulating $\text{Bi}_{1-x}\text{Sb}_x$ is that the spin polarized surface bands traverse E_F an odd number of times between $\bar{\Gamma}$ and \bar{M} [2, 12, 19]. Although this method of counting cannot be applied to Sb because it is a semimetal, since there is a direct gap at every bulk

k -point, it is meaningful to assume some perturbation, such as alloying with Bi [27] that does not significantly alter the spin splitting [Fig. 5], that pushes the bulk valence H and conduction L bands completely below and above E_F respectively without changing its Z_2 class. Under such an operation, it is clear that the spin polarized surface bands must traverse E_F an odd number of times between $\bar{\Gamma}$ and \bar{M} , consistent with the 1;(111) topological classification of Sb. This conclusion can also be reached by noticing that the spin-split pair of surface bands that emerge from $\bar{\Gamma}$ do not recombine at \bar{M} , indicative of a “partner switching” [9] characteristic of topological insulators.

In conclusion, we have mapped the spin structure of the surface bands of Sb(111) and shown that the purely surface bands located in the projected bulk gap are spin

split by a combination of spin-orbit coupling and a loss of inversion symmetry at the crystal surface. The spin polarized surface states have an asymmetric Dirac like dispersion that gives rise to its k -splitting between spin up and spin down bands at E_F . The large splitting could be due to the nature of spin-polarized photoemission and detection methods and may or may not be intrinsic in nature however, this does not affect our conclusions regarding the topological band aspects of the system. The topologically non-trivial surface band structure makes Sb(111) an especially appealing candidate for an unusual 2D Dirac protected free fermion system that exhibits antilocalization [9].

We thank F. Meier, H. Dil, J. Osterwalder for technical assistance and C.L. Kane for theoretical discussion.

-
- [1] C.L. Kane & E.J. Mele, Phys. Rev. Lett. **95**, 146802 (2005).
 [2] L. Fu and C.L. Kane, Phys. Rev. B **76**, 045302 (2007).
 [3] J.E. Moore and L. Balents, Phys. Rev. B **75**, 121306(R) (2007).
 [4] C.L. Kane & E.J. Mele, Phys. Rev. Lett. **95**, 226801 (2005).
 [5] B.A. Bernevig *et al.*, Science **314**, 1757 (2006).
 [6] M. König *et al.*, Science **318**, 766 (2007).
 [7] F.D.M. Haldane, Phys. Rev. Lett. **61**, 2015 (1988).
 [8] C. Wu *et al.*, Phys. Rev. Lett. **96**, 106401 (2006).
 [9] L. Fu *et al.*, Phys. Rev. Lett. **98**, 106803 (2007).
 [10] S. Murakami, New J. Phys. **9**, 356 (2007).
 [11] R. Roy, arXiv:cond-mat/0604211 (2006).
 [12] D. Hsieh *et al.*, Nature **452**, 970 (2008).
 [13] K. Sugawara *et al.*, Phys. Rev. Lett. **96**, 046411 (2006).
 [14] H. Höchst and C.R. Ast, J. Electron Spectrosc. Relat. Phenom. **137**, 441 (2004).
 [15] M. Hoesch *et al.*, J. Electron Spectrosc. Relat. Phenom. **124**, 263 (2002).
 [16] S. Bengió *et al.*, Surface Science **601**, 2908 (2007).
 [17] Yu. M. Koroteev *et al.*, Phys. Rev. Lett. **93**, 046403 (2004).
 [18] M. Hochstrasser *et al.*, Phys. Rev. Lett. **89**, 216802 (2002).
 [19] J. Teo, L. Fu and C.L. Kane, arXiv:0804.2664v1 [cond-mat.mes-hall] (2008).
 [20] T. Hirahara *et al.*, Phys. Rev. B **76**, 153305 (2007).
 [21] M. Hoesch *et al.*, Phys. Rev. B **69**, 241401(R) (2004).
 [22] X. Gonze *et al.*, Phys. Rev. B **44**, 11023 (1991).
 [23] L.M. Falicov and P.J. Lin, Phys. Rev. **141**, 562 (1965).
 [24] F. Meier *et al.*, Phys. Rev. B **77**, 165431 (2008).
 [25] Y. Liu and E. Allen, Phys. Rev. B **52**, 1566 (1995).
 [26] E. Kneedler, K.E. Smith, D. Skelton and S.D. Kevan, Phys. Rev. B **44**, 8233 (1991).
 [27] B. Lenoir *et al.*, Fifteenth International Conference on Thermoelectrics (Pasadena, California) 113 (IEEE, New York, 1996).